A Model For Sedimentation In Inhomogeneous Media. II. Compressibility Of Aqueous And Organic Solvents

Peter Schuck

Division of Bioengineering & Physical Science, ORS, OD, National Institutes of Health, Bethesda, Maryland 20892.

[#]Address for Correspondence:

Dr. Peter Schuck
National Institutes of Health
Bldg. 13, Rm. 3N17
13 South Drive
Bethesda, MD 20892-5766,USA
Phone: 301 435-1950
Fax: 301 480-1242
Email: pschuck@helix.nih.gov

Abstract   The effects of solvent compressibility on the sedimentation behavior of macromolecules as observed in analytical ultracentrifugation are examined. Expressions for the density and pressure distributions in the solution column are derived and combined with the finite element solution of the Lamm equation in inhomogeneous media to predict the macromolecular concentration distributions under different conditions. Independently, analytical expressions are derived for the sedimentation of non-diffusing particles in the limit of low compressibility. Both models are quantitatively consistent and predict solvent compressibility to result in a reduction of the sedimentation rate along the solution column and a continuous accumulation of solutes in the plateau region. For both organic and aqueous solvents, the calculated deviations from the sedimentation in incompressible media can be very large and substantially above the measurement error. Assuming conventional configurations used for sedimentation velocity experiments in analytical ultracentrifugation, neglect of the compressibility of water leads to systematic errors underestimating sedimentation coefficients by in the order of 1% at a rotor speeds of 45,000 rpm, but increasing to 2 – 5 % with increasing rotor speeds and decreasing macromolecular size. The proposed finite element solution of the Lamm equation can be used to take solvent compressibility quantitatively into account in direct boundary models for discrete species, sedimentation coefficient distributions or molar mass distributions. Using the analytical expressions for the sedimentation of non-diffusing particles, the ls-g*(s) distribution of apparent sedimentation coefficients is extended to the analysis of sedimentation in compressible solvents. The consideration of solvent compressibility is highly relevant when using organic solvents, but also in aqueous solvents when precise sedimentation coefficients are needed, for example for hydrodynamic modeling.

Introduction

Analytical ultracentrifugation is one of the classical first principle techniques of physical chemistry for the study of macromolecules [1, 2]. It has significant applications both in the study of biomolecules, in particular proteins and nucleic acids, as well as the study of synthetic polymers. Sedimentation equilibrium permits the determination of thermodynamic quantities, such as the molar mass and mass distribution and the characterization of reversible macromolecular interactions. The transport process observed in sedimentation velocity experiments additionally contains information, for example, on hydrodynamic shape. Because the sedimentation rate of macromolecules in the gravitational field is strongly size and shape dependent, the size-distribution of macromolecules in solution can be characterized with relatively high precision and resolution (for recent reviews, see, e.g., [3-8]).

One important consideration in ultracentrifugation experiments is the generation of pressure from the solution column in the gravitational field, which can influence the thermodynamic properties and conformation of the macromolecules under study. It is well-known that pressure can sometimes significantly affect the equilibrium constants for protein complex formation and, for example, lead to complex dissociation. More often, however, this requires pressures higher than those generated in the ultracentrifuge [2]. A more fundamental and universal pressure effect that in theory affects any sedimentation experiment is the compressibility of the solvent, since solvent density changes across the solution column will change the buoyancy of the macromolecule, and thus their sedimentation behavior. This is a practical concern primarily in sedimentation velocity experiments and sedimentation equilibrium experiments of small molecular weight solutes where higher rotor speeds are required.

Although it is commonly assumed that consideration of solvent compressibility may be

required for organic solvents but not for aqueous solvents, their compressibility is not too dissimilar: While the value of the compressibility coefficient for water is 4.59×10^{-4}/MPa, it is only twofold larger for toluene (8.96×10^{-4}/MPa), and little more than threefold larger for some of the most compressible organic solvents, such as acetone hexane. In his book, Svedberg has given tables for density changes of water across the solution column at different rotor speeds, which can amount to > 1 % at the highest rotor speed permitted by modern instrumentation [1]. This is large considering that the effects of density changes on the macromolecular sedimentation can be significantly amplified by the buoyancy of the macromolecule (a factor of 3 – 4 for proteins in aqueous solvents). Larger effects can be expected in organic solvents, which are common in analytical ultracentrifugation experiments of synthetic polymers [9-11] and supramolecular chemistry [12], but are also occasionally used in the study of biological macromolecules [13]. For example, Mosimann and Signer have described a 28 % change in buoyancy across the solution column for nitrocellulose sedimenting in acetone [14].

Only a few early publications have addressed the effect of solvent compressibility [2]. In isopycnic density gradient sedimentation, water compressibility corrections were applied in the calculation of the particle density from the equilibrium position of the band at neutral buoyancy [15]. For sedimentation velocity analysis, Fujita has considered pressure as a parameter in the general framework of centrifugal flow equations [16]. Linearized approximations for corrections to the s-values and extrapolation procedures to zero pressures were developed by Oth and Desreux [17]. Fujita has noted that such extrapolation may not be possible with precision from experimental data [16], and has derived an approximate description of the effect of hydrostatic pressure on the concentration distribution of non-diffusing particles [18]. Schachman has described the use of density gradients generated by hydrostatic pressure to measure the

compressibility of polystyrene [19]. Despite this work, overall surprisingly few theoretical studies have addressed solvent compressibility, how it affects the macromolecular concentration distribution in detail, and how it can be taken into consideration in the data interpretation. Several decades ago, this may have been, in part, due to the relative smaller effect of compressibility in aqueous solvents, which were of main interest in the biochemical application of ultracentrifugation, and due to limited instrumental precision [2]. However, with current commercial detection systems (both the absorbance scanner [20, 21] and the laser interferometry system [22-24]) and when using current data analysis techniques, the precision of the sedimentation coefficients is well in the range where the effects of solvent compressibility are significant, even for aqueous solvents.

Currently the most detailed analysis of sedimentation velocity is based on solutions of the transport equation for macromolecular diffusion and sedimentation in the gravitational field, the Lamm equation [25]. This approach permits the direct modeling of the data from the complete evolution of the macromolecular concentration distribution [26-30]. In recent years, new approximate analytical Lamm equation solutions [31, 32], and more efficient numerical algorithms for finite element solutions [33, 34] combined with algebraic noise decomposition techniques [35] have made this a routine tool for the study of macromolecular size and shape, sedimentation coefficient and molar mass distributions [36, 37], flotation coefficient distributions [38], protein self-association and hetero-association (e.g., [39-41]), non-ideal sedimentation processes in complex solvents [42], and many other processes. However, despite the increasing level of detail and statistical precision of the data analysis, solvent compressibility was so far not taken into consideration.

In the previous communication of this series, a general finite element model for

sedimentation in inhomogeneous media and its application to density gradients from sedimenting co-solutes is described [43]. In the present paper it is demonstrated how these finite element solutions of the Lamm equation can be adapted to predict and model the concentration distributions of sedimenting solutes in compressible solvents. Because many macromolecular systems exhibit a complexity that exceeds the current potential for modeling with Lamm equation solutions, a method for calculating an apparent sedimentation coefficient distribution in compressible solvents is derived. It is based on a new analytical expression in closed form for the sedimentation profiles of a non-diffusing particle in a linear compressibility approximation. These methods are implemented in the software SEDFIT (which can be downloaded from www.analyticalultracentrifugation.com) for the analysis of experimental data. Features of sedimentation in compressible aqueous and organic solvents are discussed.

Theory

The sedimentation and diffusion of a solute in the sector-shaped solution column of the

analytical ultracentrifuge was given by Lamm as

$$\frac{\partial c}{\partial t} = \frac{1}{r}\frac{\partial}{\partial r}\left[rD\frac{\partial c}{\partial r} - s\mathbf{w}^2 r^2 c\right]$$

(1)

with $c(r,t)$ denoting the concentration at a distance r from the center of rotation and at time t, ω

the angular velocity, D the diffusion coefficient, and s the sedimentation coefficient [25]. As

shown in the preceding paper, one can consider the effect of locally varying solvent viscosity

η and density ρ on the macromolecular sedimentation after transformation of the sedimentation

and diffusion coefficient to standard conditions, combined with a local buoyancy and relative

viscosity term:

$$D_{exp}(r,t) = \frac{\eta_{20,w}}{\eta(r,t)}D_{20,w} =: \alpha(r,t)D_{20,w}$$

(2a)

$$s_{exp}(r,t) = \frac{\mathbf{h}_{20,w}}{\mathbf{h}(r,t)}\left(\frac{1-\mathbf{f}'\mathbf{r}(r,t)}{1-\overline{v}\,\mathbf{r}_{20,w}}\right)s_{20,w} =: \mathbf{a}(r,t)\mathbf{b}(r,t)s_{20,w}$$

(2b)

with the partial-specific volume of the macromolecule $\overline{v}$, the apparent partial specific volume ϕ',

the standard conditions denoted with the index 20,w (for water at 20 °C), and with the

abbreviation α denoting the inverse of the relative viscosity, and with β denoting the relative

buoyancy [43]. A finite element solution of Eqs. 1 and 2 is described in the preceding paper. In

the present context, the solvent density $\rho(r,t)$ is assumed to arise only from solvent

compressibility, i.e., $\rho(r,t) = \rho(r)$. Also, in the following, the absence of a pressure dependence

of the macromolecule-solvent interactions will be assumed, and the fully solvated

macromolecule will be used as a reference under standard conditions. In this approximation, for

the present purpose the distinction between $\bar{v}$ and ϕ' in Eq. 2b can be dropped. In the case of

solvent compressibility, the relative viscosity and buoyancy coefficients α and β are independent

of time, and it is assumed in the following that the viscosity is essentially independent of

pressure (i.e., $\alpha = 1$). This case requires modifications in the propagation matrices of the

standard finite element approach, but can be solved efficiently for both the static [26, 34] and

moving frame of reference method [33].

The evaluation of Eq. 2b requires expressions for the radial dependence of the solvent

density. With the coefficient of compressibility κ, the differential density change can be

described as $d\rho = \rho\kappa dp$. The pressure change with increasing distance from the center of

rotation is related to the rotor speed and solvent density as $dp / dr = \rho\omega^2 r$. Taken together, and

with the boundary condition $\rho(m) = \rho_0$, the radial distribution of density and pressure can be

found as

$$\rho(r) = \rho_0 \left[1 - \frac{1}{2}\rho_0\omega^2\kappa\left(r^2 - m^2\right) \right]^{-1}$$

$$p(r) = -\frac{1}{\kappa}\log\left[1 - \frac{1}{2}\rho_0\omega^2\kappa\left(r^2 - m^2\right) \right]$$

(3)

(with m denoting the meniscus of the solution column). In the present paper, Eq. 3 is used to

evaluate the radial dependent solvent density. Fujita gives a considerably more complex

expression for the pressure distribution [44] which could not be reconciled (likely due to

typographical problems) with his underlying differential equation for pressure. Eq. 3 is also

slightly different from that reported in [2] (Eq. 98), which is based on an explicit expression for

the density $r(p) = r_0(1 + k\,p)$ [2, 17] as opposed to the differential $d\rho = \rho\kappa dp$ used here.

However, these differences appear only in the third term of a Taylor expansion and are very

small. In the limit of vanishing compressibility, both expressions converge to the well-known

formula for the radial dependence of the pressure

$$p(r) = \rho_0 \omega^2 (r^2 - m^2)/2 \qquad (4)$$

(Eq. 99 in [2]). A corresponding linear approximation for the density distribution at small

compressibility may be obtained by truncating the Taylor expansion of Eq. 3 to its first term

$$\boldsymbol{r}(r) = \boldsymbol{r}_0[1 + \boldsymbol{k}\boldsymbol{r}_0\boldsymbol{w}^2 (r^2 - m^2)/2] \qquad (5)$$

An important quantity for many data analysis procedures is the position $r_p(t)$ of the

sedimentation boundary and the boundary shape from sedimenting non-diffusing particles. The

boundary position can be obtained by integrating the equation of motion for a particle in the

centrifugal field, $dr_p/dt = \boldsymbol{w}^2 s r_p$, with the initial condition of $r_p(0) = m$. For homogeneous

solvents this results in the well-known expression

$$r_p(t) = m \exp\left(s\boldsymbol{w}^2 t\right) \qquad (6)$$

The corresponding boundary shape is described as a step-function with a constant plateau level

c_p that only experiences dilution with time according to the well-known expression

$$c_p(t) = c_0 \exp(-2\boldsymbol{w}^2 st) \qquad (7)$$

In compressible solvents (or inhomogeneous solvents in general) Eqs. 6 and 7 do not apply

because of the radial-dependent sedimentation rate. This makes invalid the conventional

analysis approaches that are implicitly based on Eq. 6, including the sedimentation coefficient

distributions g*(s) (in the forms of dc/dr [45], dc/dt [46, 47], and ls-g*(s) [48] as well as G(s)

[49-51]). Therefore, in the following, expressions for the sedimentation of the non-diffusing

particle through compressible solvents analogous to Eqs. 6 and 7 are sought.

Assuming the absence of other complicating factors, such as a pressure dependence of the

viscosity [2], the macromolecular frictional coefficient [44], and the partial-specific volume [19],

one can write a modified equation of motion for a non-diffusing particle in the centrifugal field as

$$\frac{dr_p}{dt} = w^2 r_p s_0 \frac{1 - \bar{v}\,r(r)}{1 - \bar{v}\,r_0} \tag{8}$$

[2]. It is possible to integrate this equation with the density distribution in the approximation of low compressibility (Eq. 5). If the particle is initially at a radius r_0, the position R at later time t is

$$R(r_0, t) = \frac{r_0 \left(\Phi + cm^2 \right)^{\frac{1}{2}} \exp\left\{ w^2 s_0 t \frac{\Phi + cm^2}{\Phi} \right\}}{\left(\Phi + c(m^2 - r_0^2) + cr_0^2 \exp\left\{ 2w^2 s_0 t \frac{\Phi + cm^2}{\Phi} \right\} \right)^{\frac{1}{2}}} \tag{9}$$

with the abbreviations $c = \bar{v}\,r_0^2\,w^2\,k/2$ and $\Phi = 1 - \bar{v}\,r_0$. In the case $r_0 = m$, Eq. 9 gives the evolution of the sedimentation boundary for non-diffusing particles $r_p(t)$, extending Eq. 6 to the case of compressible solvents in the limit of low compressibility.

The function $R(r_0, t)$ also permits calculating the shape of the plateau, which is not constant as in the incompressible case (Eq. 7) but determined by the continuous deceleration of the particles and the corresponding accumulation of material at higher radii. Let us consider the material M initially between the radii r_0 and $r_0 + \Delta r$

$$M(r_0, r_0 + \Delta r, t = 0) = \int_{r_0}^{r_0 + \Delta r} c(r, 0) r\,dr \tag{10}$$

(where $c(r,0)$ denotes the initial concentration distribution, which usually is uniform c_0), and the material M* between the propagated radial limits at a later time $R(r_0, t)$ and $R(r_0 + \Delta r, t)$:

$$M * (R(r_0, t), R(r_0 + \Delta r, t), t) = \int_{R(r_0, t)}^{R(r_0 + \Delta r, t)} c(r, t) r\,dr \tag{11}$$

In the limit of no diffusion, because $R(r_0,t)$ is a monotonous function, no particles from outside

the original interval between r_0 and $r_0+\Delta r$ can be within $R(r_0,t)$ and $R(r_0+\Delta r,t)$ at the later time,

and *vice versa*, no particles from within the original interval can escape the limits set by $R(r_0,t)$

and $R(r_0+\Delta r,t)$. It follows that $M = M^*$, and therefore Eqs. 10 and 11 are identical. Dividing the

right-hand sides of Eqs. 10 and 11 by Δr, taking the differential to the infinitesimal limits and

using the general relationship $(d/dz)\int_a^{g(z)} f(x)\,dx = f[g(z)](dg/dz)$ leads to the shape of the

concentration distribution in the 'plateau' region

$$c(R(r_0,t),t) = \frac{c(r,0)\,r_0}{R(r_0,t)\dfrac{dR(r_0,t)}{dr_0}} \tag{12}$$

The preceding considerations and the expression Eq. 12 is generally valid for the local

accumulation and dilution of non-diffusing species that migrate in a sector-shaped volume

according to any monotonous function $R(r_0,t)$. As can be easily verified, for the propagation in

homogeneous solvents with uniform loading concentration this leads to the well-known dilution

rule for the constant solvent plateau, Eq. 7. In compressible solvents with $R(r_0,t)$ as given in Eq.

9, however, the function $c(R,t)$ is not constant despite a uniform loading concentration c_0:

$$c(R(r_0,t),t) = c_0 \frac{\left(\Phi + c(m^2 - r_0^2) + cr_0^2 \exp\left\{2w^2 s_0 t \dfrac{\Phi + cm^2}{\Phi}\right\}\right)^2}{\left(\Phi + cm^2\right)^2 \exp\left\{2w^2 s_0 t \dfrac{\Phi + cm^2}{\Phi}\right\}} \quad , \quad R > r_p(t) \tag{13}$$

For the practical calculation of the 'plateau' shape, it should be noted that Eqs. 12 and 13 are

only implicitly defining the concentration distribution $c(r,t)$, because the left-hand side refers to

the concentration at the radius $R(r_0,t)$ after propagation, while the right-hand side depends on the

initial position r_0. However, this is computationally no further difficulty, as the propagation is

known, and Eq. 9 can be used to evaluate the position for which the right-hand side of Eq. 13 predicts the concentration.

The expressions Eq. 9 and 13 completely define the shape of the concentration distribution of non-diffusing particles in the limit of low compressibility. They can be used in the framework of the ls-g*(s) method [48] as a substitute of the conventional step-function (Eq. 2 in [48]) to calculate the apparent sedimentation coefficient distribution of non-diffusing particles in compressible solvents.

Results

First, as an example for the sedimentation in compressible solvents, Figure 1 shows simulated concentration profiles for 100 kDa polystyrene sedimenting in toluene (solid lines). At the bottom of a 12 mm solution column at 60,000 rpm, pressures > 30 MPa are generated, which leads to a change in the density of toluene of ~ 2.5% (or ~1.2% at in the middle of the solution column at 6.6 cm). Although this change in density may appear small, the buoyant molar mass decreases by 10% at the base (~ 5 % at the midpoint). As visible in Figure 1, this increasing buoyancy leads to a deceleration of sedimentation and consequently an accumulation of material in regions at higher radii. As a consequence, besides the shift in the boundary position, there exists no plateau region (the distributions instead show a slope that increases with time) and significantly less radial dilution is observed. As compared to the sedimentation in a homogeneous incompressible solvent (dotted lines), the changes in the concentration profiles are very substantial. The deceleration of the sedimentation boundary is qualitatively very different from any other sedimentation process, such as concentration dependent non-ideal sedimentation.

In order to validate the accuracy of the numerical results from the finite element Lamm equation solutions and the analytical expression for non-diffusing particles at low compressibility, the sedimentation profiles calculated with both methods are compared in Figure 2. Because the finite element method in the case of compressible solvents is numerically instable at $D = 0$ for both the static and moving frame of reference, very low diffusion coefficients were used, instead, to approach the limit of non-diffusing particles. Figure 2 shows the original finite element Lamm equation solutions of Figure 1 (solid line), and the results with diffusion coefficients of 10^{-8} cm^2/sec (dotted line) and 10^{-9} cm^2/sec (dash-dotted line). Also visible in Figure 2 are the analytically calculated distributions from Eq. 9 and 13 (dashed line), which are consistent with the limit of $D = 0$ approached by the series of finite element solutions. Both methods lead to consistent boundary position as well as shape of the distribution in the non-depleted region (the 'plateau' region).

When examined in more detail, slight differences between the results from the two methods were found, which are related to the limit of low compressibility (Eq. 5) on which the analytical expression is based. This introduces an underestimation of the compressibility effects at the base of the cell by approximately 2.5%. This slight underestimation of the density gradient is visible best in 'plateau' levels that are slightly lower (~ 0.2 % error) as compared to the finite element results that are based on the accurate density distribution of Eq. 3 (Figure 2, lower panel). Also, corresponding very small deviations in the boundary position were found (~ 0.002 cm), leading to errors in the s-value of below 0.1 %. As a control, when the finite element Lamm equation solutions were calculated with the same density distributions of Eq. 5, the differences between the analytical and finite element solutions in the 'plateau' region disappeared ($< 10^{-4}$, data not shown). This consistency suggests that for a given solvent density

distribution both the numerical and the analytical solutions are sufficiently accurate solutions of the Lamm equation, with deviations far below experimental precision. The small differences observed in the lower panel of Figure 2 can be fully attributed to the assumption of small compressibility which is underlying the analytical expressions for sedimentation of non-diffusing particles.

Sedimentation in compressible solvents was implemented in SEDFIT fully compatible with the continuous sedimentation coefficient and molar mass distribution models, c(s) and c(M), respectively. This is shown in Figure 3, where the data from Figure 1 (after adding 0.01 normally distributed noise) were modeled as a sedimentation coefficient distribution from independently sedimenting macromolecular species with unknown weight-average frictional ratio f/f_0. The sedimentation coefficient distribution results in a single peak at the correct sedimentation coefficient of 0.8 S. The non-linear regression of the weight-average frictional ratio f/f_0 converged to a value of 2.82, virtually identical to that underlying the simulation. As is the case in with data from the corresponding sedimentation in a homogeneous solvent, the weight-average frictional ratio is well-determined and permits here the calculation of both c(s) and c(M) distributions (as outlined elsewhere for homogeneous solvents, a reliable c(M) distribution cannot be calculated if either f/f_0 is not well determined or if more than one peak is obtained in c(s)) [51].

In many cases where the macromolecular sedimentation is more complex, for example, in multi-component systems with attractive or repulsive interactions, it can be desirable to achieve a more model-independent description of the sedimentation process. This can be accomplished, for example, by using apparent sedimentation coefficient distributions, or by reducing the analysis to the determination of the weight-average sedimentation coefficient. In compressible

solvents, this is complicated by the absence of a plateau region. This does not allow to define the weight-average sedimentation coefficient through second moment considerations [2]. Further, the position-dependent buoyancy also makes problematic the application of the sedimentation coefficient distributions that utilize the laws for ideal sedimentation of a non-diffusing species in homogeneous solvents. If solvent compressibility is ignored, the g*(s) method leads to a slightly asymmetric apparent sedimentation coefficient distribution with a peak at a too small s-value (dashed line in Figure 4). The integral sedimentation coefficient distribution G(s) from the van Holde-Weischet method [49] is also centered at too small s-values, and would wrongly suggest the presence of repulsive non-ideal sedimentation (dotted line in Figure 4). In both cases, the resulting distribution and the apparent weight-average s-value will depend on the data subset used for the analysis.

Two methods are available for calculating the apparent sedimentation coefficient distribution taking solvent compressibility into account. The first method is based on the analytical expressions Eqs. 9 and 13 substituting the conventional step-functions in the ls-g*(s) method [48] (Figure 4, solid line). This makes the assumption of low compressibility since it uses the linearized density distribution of Eq. 5. The second method is based on an exact description of the solvent density distribution, but approximates the limit of no diffusion of g*(s) by very low diffusion, which is achieved in the c(s) method when fixing the weight-average frictional ratio to a very large number [51] (circles in Figure 4). Both approaches lead to consistent results. Importantly, these distributions are also very similar to that obtained for simulated sedimentation in incompressible solvents under otherwise identical conditions. This shows that the use of either method for calculating g*(s) in compressible solvents (in particular the computationally more efficient modified ls-g*(s) method) provides a very effective and

simple way of accounting for solvent compressibility. Further, like the ordinary c(s) and ls‑g*(s)

distributions, their integration report a weight-average s at the correct value, independent of the

data subsets considered.

In the following, the effects of the compressibility of water on the sedimentation velocity

analysis are examined. Although water is less compressible than most organic solvents, the

compressibility coefficient is still large enough to significantly influence macromolecular

sedimentation. Figure 5 shows the calculated concentration distributions of a 50 kDa protein

with an s-value of 4 S sedimenting at 60,000 rpm (solid lines). Compared to the sedimentation

in an ideal incompressible solvent (dashed lines), the sedimentation boundary exhibits a

retardation and distortion that is very significant. The maximal difference between the

concentration distribution in compressible water versus incompressible solvent are > 0.05, which

is approximately 10fold above the experimental error in data acquisition. If the compressibility

of water is ignored, the analysis with a single species model leads to an error in the molar mass

and sedimentation coefficient by +3 % and – 1.9%, respectively. (These values refer to a fit with

unknown meniscus position and baseline signal; if additionally systematic time‑invariant and

radial‑invariant noise contributions are permitted, the errors in M and s are 1.4% and 0.9%,

respectively.) As shown in Figure 5, the residuals of such a fit are clearly systematic, and show

the largest deviation close to the meniscus.

The underestimation of the s-value and the magnitude and pattern of residuals when

ignoring water compressibility were found to be qualitatively similar in simulations for proteins

of different sizes. However, as shown in Figure 6 (top panel), the errors made if water

compressibility is ignored sharply increases with smaller molar mass of the solute. (The precise

influence on the result with the impostor model does also depend on other parameters, such as

fitting limits and baseline parameters considered.) This error decreases with decreasing solution column (Figure 6, middle panel) and with decreasing rotor speed (Figure 6, lower panel). For example, for ordinary solution column heights of 12 mm and a protein of 100 kDa, water compressibility influences the sedimentation coefficients by more than 1 % at rotor speeds larger than 45,000 rpm. Larger effects were found for smaller macromolecules.

Discussion

The effects of solvent compressibility on macromolecular sedimentation behavior can be quite large. This has been known for a long time in the area of polymer characterization with organic solvents, but has generally not been appreciated for aqueous systems. Although the compressibility of water is less than most organic solvents, it is not qualitatively and not much quantitatively different. The present calculations show that for sedimentation velocity experiments it cannot be neglected in either case. This is in line with observations made several decades ago. In 1940, Svedberg recommended the consideration of solvent compressibility for organic solvents, but for aqueous solvents only at high rotor speeds and solution columns [1]. In 1959, Schachman noted that large gains in experimental precision will make pressure corrections more important [2]. Despite even more substantial technological and computational improvements increasing the sensitivity and precision of sedimentation velocity in the recent years, little attention has been paid to solvent compressibility for either organic or aqueous solvents.

One theoretical difficulty of describing sedimentation in compressible solvents is that the Lamm equation is based on the assumption of a constant partial-specific volumes for all components, and that it describes the sedimentation and diffusion coefficients in a volume-fixed frame of reference [52]. Without these assumptions, currently no rigorous theory for practical flow equations are known that describe macromolecular sedimentation in compressible solvents [52]. The approximation used in the present work relies on the solvent compressibility being small enough so that solvent and macromolecular flows do not significantly change the center of volume of the mixture, and the volume-based reference frame on the Lamm equation is close to the cell-based frame in which the measurement takes place. Because of small absolute changes

in the partial-specific volume of the solvent and at dilute macromolecular conditions this appears

to be a reasonable approximation. (For example, at 1 mg/ml polystyrene in toluene solution at

50,000 rpm in a 12 mm solution column, the fractional volume expansion due to complete

sedimentation of the polymer into the compressed regions of the cells can be estimated to be in

the order of 10^{-5}.)

In the present paper, two new approaches are described to describe sedimentation under

consideration of the solvent compressibility. The first is based on numerical solutions of the

Lamm equation, using the finite-element framework described in the accompanying paper for

sedimentation in inhomogeneous media [43]. The second approach is a new analytical solution

of the Lamm equation for non-diffusing particles in the approximation of low compressibility.

The approximation of low compressibility leads to errors that in practice for ordinary solvents

will be far below the detection limit. Both methods currently are limited by neglecting the

compressibility of the macromolecule itself [2], and the pressure dependence of the solvent

viscosity. However, if required the consideration of the two latter factors could be easily

included in the framework of the finite element model. The numerical solution of the Lamm

equation permits the direct boundary analysis with models for independent 'ideally' sedimenting

species, diffusion-deconvoluted sedimentation coefficient distributions c(s), and can in principle

be combined with finite element models of interacting species. The analytical solutions for non-

diffusing particles, on the other hand, permit a more 'model-free' description of the

sedimentation process in the form of a ls-g*(s) distribution, which may be more appropriate, for

example, for strongly concentration-dependent polydisperse polymer samples and could be

coupled with extrapolation procedures to infinite dilution [53]. Together, both approaches

extend the conventional tools for sedimentation velocity analysis to account for solvent

compressibility. They are applicable to the modeling of experimental data in the software SEDFIT.

The main feature of the predicted concentration distributions in compressible solvents is a decrease of the sedimentation velocity along the solution column, which leads to a deceleration of the boundary and to an increase of the macromolecular concentration with radius. This is consistent with earlier calculations in the absence of diffusion [2, 18]. The deceleration is due to the increased buoyancy in regions of higher pressure and higher solvent density. The difference can be very significant. In the example simulated here, the sedimentation of polystyrene in toluene, it amounts to 10%, but it can be significantly larger for solvents with higher compressibility (such as acetone or hexane) and/or solutes that are closer in density to the solvent [14, 19]. Correspondingly, the effects on the boundary shape can also be quite large (Figures 1 and 2).

It should be noted that the qualitative observation of an increasing concentration with radius in the 'plateau' region is not sufficient to diagnose the presence of solvent compressibility effects, as a visually 'sloping plateau' may originate also from the sedimentation of small populations of aggregates with a very broad size-distribution, the sedimentation of a very small species (e.g., a buffer component that contributes to the detected signal) or optical artifacts. (Interestingly, the plateau patterns from compressibility correlate more with an ideally sedimenting very small species than with a broad distribution of large species; we did not observe artificial peaks at large s-values in the c(s) analysis if compressibility was unaccounted for, rather a small apparent increase in c(s) at the limit of the smallest s-value, data not shown). However, a much better qualitative feature for solvent compressibility is the deceleration of the sedimentation boundary, which produces large residuals with any model if compressibility is not

accounted for. Fortunately, as a physical process that is independent of the sample under study, the extent of solvent compressibility is very predictable. As described in the present paper, its effects can be calculated from first principles and quantitatively incorporated in the sedimentation model.

The neglect of the solvent compressibility will lead to significant errors. This is not surprising for organic solvents. More unexpectedly, effects of compressibility of water can also be substantial. According to the presented calculations, the neglect of compressibility will lead to an underestimation of the sedimentation coefficient by 1% or more for relatively large proteins studied at rotor speeds over 45,000 rpm, and larger deviations are predicted for smaller proteins and peptides and at higher rotor speeds (e.g., 2 – 2.5 % for a 10kDa protein at 50,000 – 60,000 rpm). Such deviations are significantly above the measurement errors. The present estimates assume protein partial specific volumes of 0.73 ml/g, but larger effects will be seen in proteins, e.g., lipoproteins, with densities closer to the solvent. But even for proteins of common partial-specific volume, the hydrostatic compressibility of water can be of practical importance, for example, when comparing sedimentation coefficients obtained at different rotor speeds, or when precise absolute sedimentation coefficients are required for hydrodynamic modeling [54-57].

References

[1] T. Svedberg and K. O. Pedersen (1940) Die Ultrazentrifuge, Theodor Steinkopff, Dresden.

[2] H. K. Schachman (1959) Ultracentrifugation in Biochemistry, Academic Press, New York.

[3] G. Rivas, W. Stafford and A. P. Minton, Characterization of heterologous protein-protein interactions via analytical ultracentrifugation, Methods: A Companion to Methods in Enzymology 19 (1999) 194-212

[4] J. Liu and S. J. Shire, Analytical ultracentrifugation in the pharmaceutical industry, J Pharm Sci 88 (1999) 1237-41

[5] F. Arisaka, Applications and future perspectives of analytical ultracentrifugation, Tanpakushitsu Kakusan Koso 44 (1999) 82-91

[6] T. M. Laue and W. F. I. Stafford, Modern applications of analytical ultracentrifugation., Annu. Rev. Biophys. Biomol. Struct. 28 (1999) 75-100

[7] P. Schuck and E. H. Braswell (2000) *in* Current Protocols in Immunology (J. E. Coligan, A. M. Kruisbeek, D. H. Margulies, E. M. Shevach and W. Strober, Eds.), pp. 18.8.1-18.8.22, John Wiley & Sons, New York.

[8] J. Lebowitz, M. S. Lewis and P. Schuck, Modern analytical ultracentrifugation in protein science: a tutorial review, Protein Sci 11 (2002) 2067-79

[9] H. Suzuki (1992) *in* Analytical Ultracentrifugationin Biochemistry and Polymer Science (S. E. Harding, A. J. Rowe and J. C. Horton, Eds.), pp. 568-592, The Royal Society of Chemistry, Cambridge.

[10] D. N. Pinder, T. Ueleni and J. A. Lewis, Comparison of diffusion coefficients obtained from ternary polymer solutions using dynamic light scattering and ultracentrifugation, J. Molecular Structure 383 (1996) 107-115

[11] M. D. Lechner and W. Mächtle, Characterization of nanoparticles., Materials Science Forum 352 (2000) 87-90

[12] D. Schubert, C. Tziatzios, P. Schuck and U. S. Schubert, Characterizing the solution properties of supramolecular systems by analytical ultracentrifugation., Chem. Eur. J. 5 (1999) 1377-1383

[13] K. K. W. Wong, H. Cölfen, N. T. Whilton, T. Douglas and S. Mann, Synthesis and characterization of hydrophobic ferritin proteins, J. Inorganic Biochemistry 76 (1999) 187-195

[14] H. Mosimann and R. Signer, Helv. Chim. Acta. 27 (1944) 1123

[15] J. Vinograd and J. E. Hearst, Equilibrium sedimentation of macromolecules and viruses in a density gradient, Fortschritte der Chemie organischer Naturstoffe 20 (1962) 372-422

[16] H. Fujita (1962) Mathematical Theory of Sedimentation Analysis, Academic Press, New York.

[17] J. Oth and V. Desreux, Bull. Soc. Chim. Belges 63 (1954) 133

[18] H. Fujita, J. Am. Chem. Soc. 63 (1956) 1092

[19] P. Y. Cheng and H. K. Schachman, The effect of pressure on sedimentation, and compressibility measurements in teh ultracentrifuge., J. Am. Chem. Soc. 77 (1954) 1498-1501

[20] S. Hanlon, K. Lamers, G. Lauterbach, R. Johnson and H. K. Schachman, Ultracentrifuge studies with absorption optics. I. An automatic photoelectric scanning absorption system, Arch. Biochem. Biophys. 99 (1962) 157-174

[21] R. Giebeler (1992) *in* Analytical Ultracentrifugation in Biochemistry and Polymer Science. (S. E. Harding, A. J. Rowe and J. C. Horton, Eds.), pp. 16-25, The Royal Society of Chemistry, Cambridge, U.K.

[22] T. M. Laue, R. A. Domanik and D. A. Yphantis, Rapid precision interferometry for the analytical ultracentrifuge. I. A laser controller based on a phase-lock-loop circuit, Anal Biochem 131 (1983) 220-31

[23] D. A. Yphantis, T. M. Laue and I. Anderson, Rapid precision interferometry for the analytical ultracentrifuge. II. A laser controller based on a rate-multiplying circuit, Anal Biochem 143 (1984) 95-102

[24] T. M. Laue, An on-line interferometer for the XL-A ultracentrifuge, Prog. Coll. Polym. Sci. 94 (1994) 74-81

[25] O. Lamm, Die Differentialgleichung der Ultrazentrifugierung, Ark. Mat. Astr. Fys. 21B(2) (1929) 1-4

[26] J.-M. Claverie, H. Dreux and R. Cohen, Sedimentation of generalized systems of interacting particles. I. Solution of systems of complete Lamm equations, Biopolymers 14 (1975) 1685-1700

[27] L. A. Holladay, An approximate solution to the Lamm equation, Biophys. Chem. 10 (1979) 187-190

[28] J. R. Cann and G. Kegeles, Theory of sedimentation for kinetically controlled dimerization reactions, Biochemistry 13 (1974) 1868-1874

[29] D. J. Cox and R. S. Dale (1981) *in* Protein-protein interactions. (C. Frieden and L. W. Nichol, Eds.), Wiley, New York.

[30] G. P. Todd and R. H. Haschemeyer, General solution to the inverse problem of the differential equation of the ultracentrifuge, Proc Natl Acad Sci U S A 78 (1981) 6739-43

[31] J. S. Philo, An improved function for fitting sedimentation velocity data for low molecular weight solutes, Biophys. J. 72 (1997) 435-444

[32] J. Behlke and O. Ristau, A new approximate whole boundary solution of the Lamm differential equation for the analysis of sedimentation velocity experiments, Biophys Chem 95 (2002) 59-68

[33] P. Schuck, Sedimentation analysis of noninteracting and self-associating solutes using numerical solutions to the Lamm equation, Biophys. J. 75 (1998) 1503-1512

[34] P. Schuck, C. E. MacPhee and G. J. Howlett, Determination of sedimentation coefficients for small peptides, Biophys. J. 74 (1998) 466-474

[35] P. Schuck and B. Demeler, Direct sedimentation analysis of interference optical data in analytical ultracentrifugation., Biophys. J. 76 (1999) 2288-2296

[36] P. Schuck, Size distribution analysis of macromolecules by sedimentation velocity ultracentrifugation and Lamm equation modeling, Biophys. J. 78 (2000) 1606-1619

[37] D. M. Hatters, L. Wilson, B. W. Atcliffe, T. D. Mulhern, N. Guzzo-Pernell and G. J. Howlett, Sedimentation analysis of novel DNA structures formed by homo-oligonucleotides, Biophys. J. 81 (2001) 371-381

[38] M. A. Perugini, P. Schuck and G. J. Howlett, Differences in the binding capacity of human apolipoprotein E3 and E4 to size-fractionated lipid emulsions, Eur J Biochem 269 (2002) 5939-3949

[39] D. Madern, C. Ebel, M. Mevarech, S. B. Richard, C. Pfister and G. Zaccai, Insights into the molecular relationships between malate and lactate dehydrogenases: structural and

biochemical properties of monomeric and dimeric intermediates of a mutant of tetrameric L-[LDH-like] malate dehydrogenase from the halophilic archaeon Haloarcula marismortui, Biochemistry 39 (2000) 1001-10

[40] Z. F. Taraporewala, P. Schuck, R. F. Ramig, L. Silvestri and J. T. Patton, Analysis of a temperature-sensitive mutant rotavirus indicates that NSP2 octamers are the functional form of the protein, J Virol 76 (2002) 7082-93

[41] W. F. Stafford (2000) *in* Methods Enzymol. (M. L. Johnson, J. N. Abelson and M. I. Simon, Eds.), Vol. 323, pp. 302-25., Academic Press, New York.

[42] A. Solovyova, P. Schuck, L. Costenaro and C. Ebel, Non-ideality by sedimentation velocity of halophilic malate dehydrogenase in complex solvents, Biophysical Journal 81 (2001) 1868-80

[43] P. Schuck, submitted *(this is the preceding paper of this series)*

[44] H. Fujita, Effects of hydrostatic pressure upon sedimentation in the ultracentrifuge., J. Am. Chem. Soc. 78 (1956) 3598-3604

[45] R. Signer and H. Gross, Ultrazentrifugale Polydispersitätsbestimmungen an hochpolymeren Stoffen, Helv. Chim. Acta 17 (1934) 726

[46] W. F. Stafford, Boundary analysis in sedimentation transport experiments: a procedure for obtaining sedimentation coefficient distributions using the time derivative of the concentration profile, Anal. Biochem. 203 (1992) 295-301

[47] J. S. Philo, A method for directly fitting the time derivative of sedimentation velocity data and an alternative algorithm for calculating sedimentation coefficient distribution functions, Anal. Biochem. 279 (2000) 151-163

[48] P. Schuck and P. Rossmanith, Determination of the sedimentation coefficient distribution by least-squares boundary modeling, Biopolymers 54 (2000) 328-341

[49] K. E. van Holde and W. O. Weischet, Boundary analysis of sedimentation velocity experiments with monodisperse and paucidisperse solutes., Biopolymers 17 (1978) 1387-1403

[50] B. Demeler, H. Saber and J. C. Hansen, Identification and interpretation of complexity in sedimentation velocity boundaries, Biophys J 72 (1997) 397-407

[51] P. Schuck, M. A. Perugini, N. R. Gonzales, G. J. Howlett and D. Schubert, Size-distribution analysis of proteins by analytical ultracentrifugation: strategies and application to model systems, Biophys J 82 (2002) 1096-1111

[52] H. Fujita (1975) Foundations of ultracentrifugal analysis, John Wiley & Sons, New York.

[53] N. Gralén and G. Lagermalm, A contribution to the knowledge of some physico-chemical properties of polystyrene., J. Phys. Chem. 56 (1952) 514-523

[54] J. Garcia De La Torre, M. L. Huertas and B. Carrasco, Calculation of hydrodynamic properties of globular proteins from their atomic-level structure, Biophys J 78 (2000) 719-30

[55] M. Rocco, B. Spotorno and R. R. Hantgan, Modeling the alpha IIb beta 3 integrin solution conformation, Protein Sci 2 (1993) 2154-66

[56] P. J. Morgan, S. C. Hyman, O. Byron, P. W. Andrew, T. J. Mitchell and A. J. Rowe, Modeling the bacterial protein toxin, pneumolysin, in its monomeric and oligomeric form, J Biol Chem 269 (1994) 25315-20

[57] O. Byron, Hydrodynamic bead modeling of biological macromolecules, Methods Enzymol 321 (2000) 278-304

[58] D. R. E. Lide (2003) Handbook of Chemistry and Physics, CRC Press, Boca Raton.

Figure Legends

Figure 1: Effects of compressibility in organic solvents: Calculated sedimentation profiles for polystyrene with a molar mass of 100 kDa ($\bar{v} = 0.917$ ml/g, $s_{20,w} = 0.8$ S) in toluene ($\rho = 0.867$ g/ml, $\kappa = 8.96 \times 10^{-4}$/MPa, $\eta = 0.56$ mPa$\times$s [58]) at a rotor speed of 60,000 rpm, and a temperature of 25 °C. The concentration distributions are shown in time intervals of 1500 sec. For comparison, the dotted lines indicate the sedimentation profiles for an incompressible solvent under otherwise identical conditions.

Figure 2: Comparison of analytical Lamm equation solution for non-diffusing particles in the low compressibility approximation with the finite element Lamm equation solution. Top Panel: Sedimentation profiles calculated under the condition of Figure 1 for polystyrene in toluene (solid line). Finite element Lamm equation solutions calculated with lower diffusion coefficient under otherwise identical conditions are shown as dotted line for $D_{20,w}$ of 10^{-8} cm^2/sec and dash-dotted line for $D_{20,w}$ of 10^{-9} cm^2/sec, respectively. The concentration distributions for a non-diffusing species calculated analytically via Eq. 9 and 13 is shown as dashed line. Lower Panel: Same distributions at higher magnification in the 'plateau' region.

Figure 3: Sedimentation coefficient distributions from the analysis of the sedimentation data in compressible solvents shown in Figure 1. (Normally distributed noise of magnitude 0.01 was added.) The sedimentation coefficient distribution c(s) with deconvoluted diffusion (solid line) was calculated with maximum entropy regularization on a confidence level of 0.9 [36], and with non-linear regression of the weight-average frictional ratio f/f$_0$ [51]. Because f/f$_0$ was well-determined and a single peak is observed in c(s), the result can be transformed to a molar mass

distribution c(M) (inset).

Figure 4: Results from alternative sedimentation coefficient distributions applied to the data in

Figure 1. Distributions calculated without considering solvent compressibility: g*(s) distribution

(calculated as ls-g*(s) [48] with the data subset from 7500 to 9000 seconds) (dashed line), and

van-Holde-Weischet distribution G(s) [49] applied to the data in Figure 1 (without noise and in

time intervals of 300 sec) (dotted vertical line). Two approaches for calculating the apparent

sedimentation coefficient distribution g*(s) with solvent compressibility are shown: low-

compressibility approximation using the analytical expression for the sedimentation profiles of

non-diffusing particles as kernel in the ls-g*(s) method (solid line); and a low-diffusion

approximation from a c(s) distribution with fixed friction ratio at $f/f_0 = 20$ (circles). For

comparison, the result of a conventional g*(s) distribution obtained from the sedimentation in a

homogeneous incompressible solvent under otherwise identical conditions (crosses).

Figure 5: Calculated effect of compressibility of water. Top Panel: Sedimentation profiles were

simulated for a 50 kDa protein with $s_{20,w} = 4$ S at unit loading concentration, sedimenting at a

rotor speed of 60,000 rpm in water with a compressibility coefficient of 4.59×10^{-4}/MPa [58].

Distributions are shown from 900 sec in intervals of 1500 sec (solid lines). For comparison, the

sedimentation profiles in an incompressible medium under otherwise identical conditions are

shown as dashed lines. Lower Panel: Residuals of modeling the sedimentation data without

considering compressibility: A single species model was fitted to the scans starting at 300 sec to

11,400 sec in 300 sec intervals, allowing for an unknown meniscus position and baseline signal.

The residuals of the best-fit are shown (in units of loading concentration), which has a root-

mean-square deviation of 0.0054, and leads to an overestimation of the molar mass by 3% and an underestimation of the sedimentation coefficient by 1.9%. The inset shows the residuals bitmap (scaled to represent residuals of ± 0.05 from black to white) for the fitted radius range of 6.007 cm to 7.133 cm.

Figure 6: Relative errors of the estimates for the sedimentation coefficient (squares) and molar mass (circles) in the analysis of a single non-interacting species if the compressibility of water is ignored. Top Panel: Sedimentation profiles were simulated with a value of the compressibility coefficient of of 4.59×10^{-4}/MPa [58], and analyzed by non-linear regression with a single-species model without compressibility. Results are based on a 12 mm solution column, a rotor speed of 60,000 rpm, and simulated sedimentation of molecules with 500 Da and 0.15 S, 750 Da and 0.23 S, 1 kDa and 0.3 S, 3 kDa and 0.6 S, 10 kDa and 1.5 S, 50 kDa and 4 S, 100 kDa and 7 S, and 200 kDa and 10 S, respectively. Middle Panel: Influence of the solution column height. Sedimentation profiles were simulated for a 10 kDa protein with a sedimentation coefficient of 1.5 S at 60,000 rpm with a compressibility coefficient of of 4.59×10^{-4}/MPa [58]. Shown are the relative errors in the sedimentation coefficient when the data were modeled as a single species without considering compressibility. Lower Panel: Influence of the rotor speed for a 10 kDa protein with 1.5 S (squares), and for a 100 kDa protein with 7 S (circles). The vertical line indicates the limit of the rotor speed for current commercial analytical rotors. Simulations were based on a solution column of 12 mm.
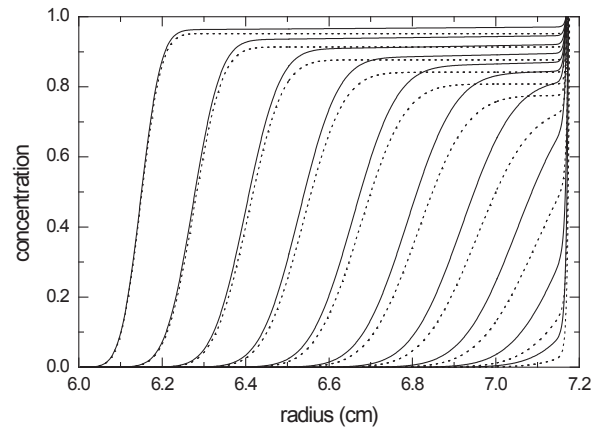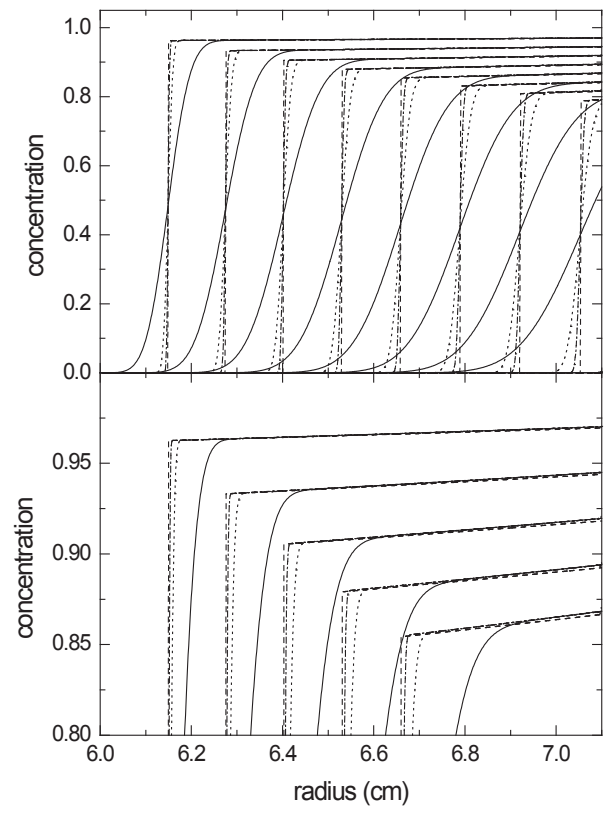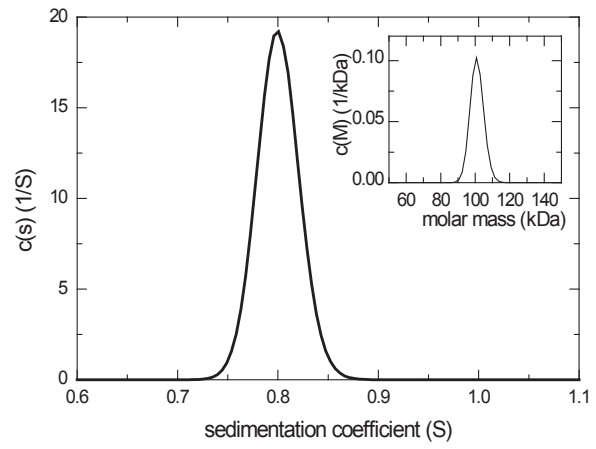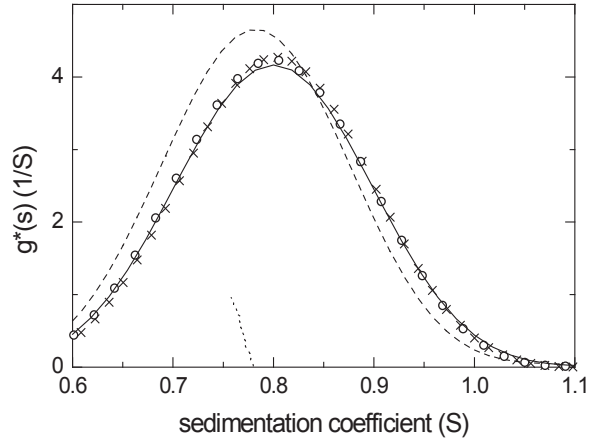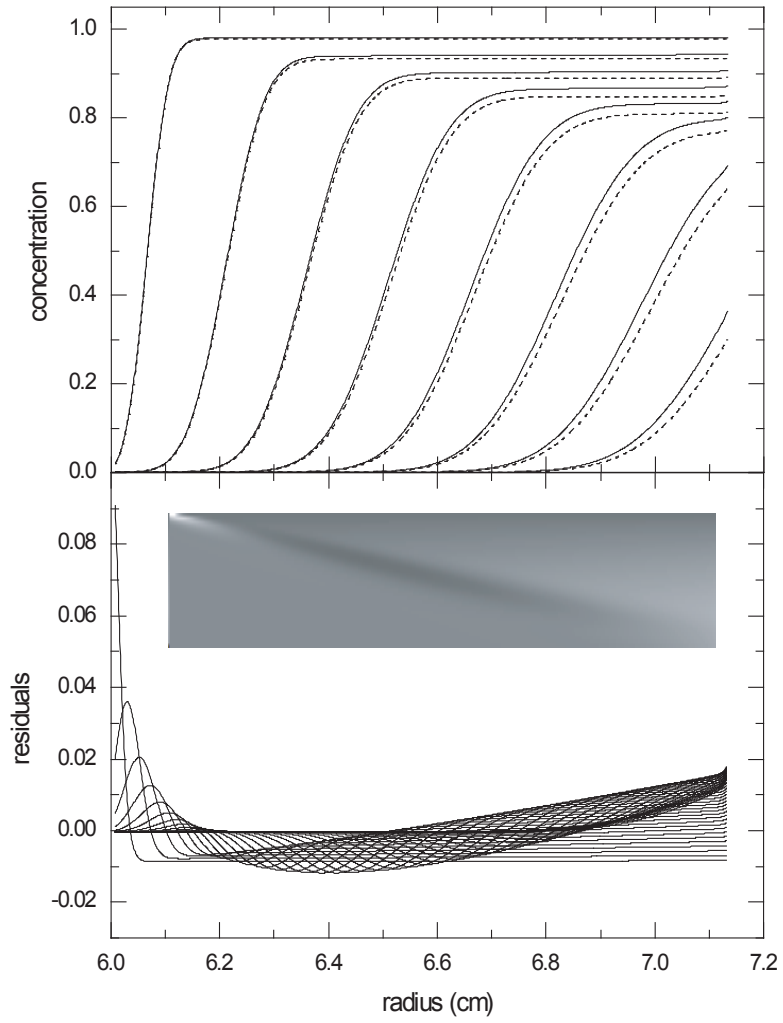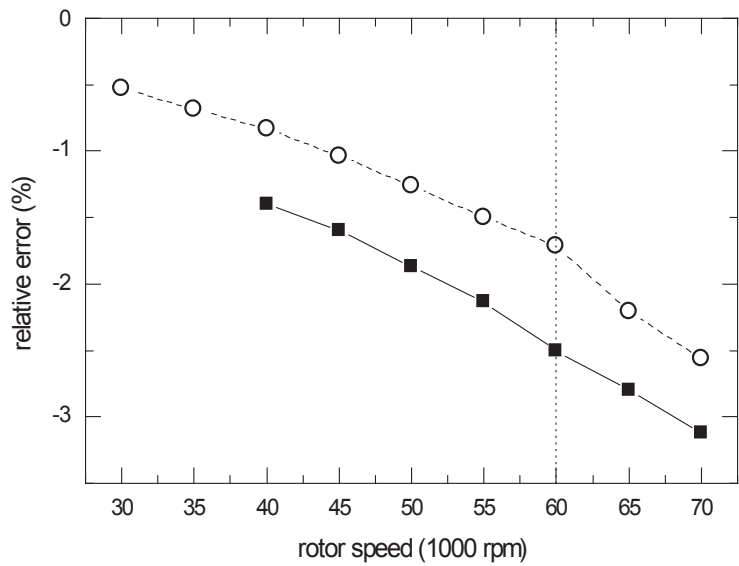
Figure 1

Figure 2

Figure 3

Figure 4

Figure 5

Figure 6